https://doi.org/10.5194/amt-2020-394
Preprint. Discussion started: 26 October 2020

Atmospheric Measurement Techniques Discussions

Observation of Cirrus Clouds with GLORIA during the WISE Campaign: Detection Methods and Cirrus Characterization

Irene Bartolome Garcia[1], Reinhold Spang[1], Jörn Ungermann[1], Sabine Griessbach[2], Martina Krämer[1], Michael Höpfner[3], and Martin Riese[1]

[1]Institute für Energie and Klimaforschung (IEK-7), Forschungszentrum Jülich GmbH, 52428 Jülich, Germany
[2]Jülich Supercomputing Centre (JSC), Forschungszentrum Jülich GmbH, 52428 Jülich, Germany
[3]Institute of Meteorology and Climate Research, Karlsruhe Institute of Technology, 76021 Karlsruhe, Germany

Correspondence: Irene Bartolome Garcia (i.bartolome@fz-juelich.de)

Abstract. Cirrus clouds contribute to the general radiation budget of the Earth, playing an important role in climate projections. Of special interest are optically thin cirrus clouds close to the tropopause due to the fact that their impact is not yet well understood. Measuring these clouds is challenging as both high spatial resolution as well as a very high detection sensitivity are needed. These criteria are fulfilled by the infrared limb sounder GLORIA (Gimballed Limb Observer for Radiance Imaging of the Atmosphere). This study presents a characterization of observed cirrus clouds using the data obtained by GLORIA aboard the German research aircraft HALO during the WISE (Wave-driven ISentropic Exchange) campaign in September/October 2017. We developed an optimized cloud detection method and derived macro-physical characteristics of the detected cirrus clouds such as cloud top height, cloud top bottom height, vertical extent and cloud top position with respect to the tropopause. The fraction of cirrus clouds detected above the tropopause is in the order of 13 % to 27 %. In general, good agreement with the clouds predicted by the ERA5 reanalysis data-set is obtained. However, cloud occurrence is ≈50 % higher in the observations for the region close to and above the tropopause. Cloud bottom heights are also detected above the tropopause. However, considering the uncertainties, we cannot confirm the formation of unattached cirrus layers above the tropopause.

1 Introduction

High clouds, composed of ice crystals, are formed in the upper troposphere, where the temperatures are lower than -30°C. It is possible to differentiate three genera: cirrus, cirrocumulus and cirrostratus. The first one consists of white delicate filaments, the second one of banks of small, white flakes and the third one of translucent cloud veils. According to Sassen et al. (2008), these high clouds cover 16.7 % of the Earth's surface on average. All these clouds (from now on simply cirrus) are important, due to their frequent occurrence and their effect on the radiative budget of the Earth (Liou, 1986). Cirrus clouds are rather transparent to incoming solar radiation, but absorb IR radiation from below and emit less to space due to the low temperature of their environment. Thus, they influence the amount of solar radiative energy received and also the loss of energy. These clouds

https://doi.org/10.5194/amt-2020-394
Preprint. Discussion started: 26 October 2020


Atmospheric Measurement Techniques Discussions

are challenging to measure because they can appear in multilayered cloud systems and they can be optically very thin, which complicates its detection by nadir sounders that are the typical operational weather satellites. Whereas in-situ measurements are capable of detecting the thinnest clouds, they only capture a temporally and spatially limited snapshot. Because of these difficulties, and despite being the subject of many studies, processes related to cirrus clouds are still not well understood and cause large uncertainties in climate projections (IPCC, 2013). Important factors influencing these uncertainties are ice water content, crystal number concentration and size distribution (Fusina et al., 2007). Other important factors that are problematic to determine are exact altitude and thickness. According to Sassen and Cho (1992) cirrus clouds are defined as (optically) thick for an optical depth $\tau > 0.3$, (optically) thin for $0.03 < \tau < 0.3$ and subvisible (SVC) for $\tau < 0.03$ in the visible wavelength region.

Of special interest is the effect of cirrus clouds in the upper troposphere / lowermost stratosphere (UTLS) region. Even small changes in the concentration of water vapor in this region affect the radiative forcing of the atmosphere (Riese et al., 2012). The presence of cirrus clouds above the tropopause, that will evaporate as soon as they experience a temperature increase and thus contribute to the water vapor budget, is still an ongoing discussion. Pan and Munchak (2011) show the importance of the employed tropopause definition and usage of tropopause relative coordinates for this kind of analysis. Using the same set of measurements from the Cloud and Aerosol Lidar (CALIOP) as Dessler (2009), they find less occurrences above the tropopause and consider that there is not enough evidence of clouds above the tropopause in mid-latitudes. Spang et al. (2015) use the measurements from the Cryogenic Infrared Spectrometers and Telescopes (CRISTA) and ERA-Interim temperature fields for the determination of the local tropopause and conclude that there is a significant number of occurrences in the lowermost stratosphere at mid and high latitudes. A recent study with the Michelson Interferometer for Passive Atmospheric Sounding (MIPAS) and Cloud-Aerosol Lidar and Infrared Pathfinder Satellite Observations (CALIPSO) by Zou et al. (2020) finds that CALIPSO observes occurrence frequencies of about $2\,\%$ of stratospheric cirrus clouds at mid and high latitudes and $4 - 5\,\%$ for MIPAS in middle latitudes. Other studies based on measurements by ground-based LIDARs show thin cirrus that are unambiguously located in the lowermost stratosphere (Keckhut et al., 2005). In the analysis of Goldfarb et al. (2001) using data from northern mid-latitudes, cirrus cloud tops often occur at the tropopause and SVC constitute $23\,\%$ of the total occurrences of cirrus clouds.

Detection of optically thin cirrus clouds and SVCs is a challenge due to the needed high vertical resolution and high sensitivity. This type of clouds is often invisible to nadir viewing instruments, but detectable by limb viewing instruments due to the longer path of the line-of-sight through the cirrus. Spang et al. (2008) detect optically thin clouds with ice water content (IWC) down to $0.01\,\mathrm{ppmv}$ using the airborne limb instrument Cryogenic Infrared Spectrometers and Telescopes for the Atmosphere - New Frontiers (CRISTA-NF). This IWC value matches the lower limit of the expected IWC for mid-latitude cirrus clouds $0.01 - 200\,\mathrm{ppmv}$ (Luebke et al., 2016). Our study uses data from the airborne Gimballed Limb Observer for Radiance Imaging of the Atmosphere (GLORIA) instrument (Riese et al., 2014; Friedl-Vallon et al., 2014). This instrument possesses the technical characteristics necessary for the detection of thin cirrus and SVCs. It has a spatial resolution of $140\,\mathrm{m} \times 140\,\mathrm{m}$ (horizontal sampling $\times$ vertical sampling) at a tangent point altitude of $10\,\mathrm{km}$ for a flight altitude of $15\,\mathrm{km}$. It measures in the infrared spectral region between 780 and $1400\,\mathrm{cm}^{-1}$ and its long line-of-sight provides sufficient sensitivity to low ice concentrations.

https://doi.org/10.5194/amt-2020-394
Preprint. Discussion started: 26 October 2020


Atmospheric Measurement Techniques Discussions

Our work analyzes the cirrus measured by GLORIA during the Wave-driven ISentropic Exchange (WISE) campaign in September/October 2017 with the purpose of obtaining more information about the nature of cirrus and thus, improve the understanding of their formation processes. The analysis includes the macro-physical properties of cirrus clouds, i.e., cloud top height (CTH), cloud bottom height (CBH), vertical extent and their position with respect to the tropopause.

2 Datasets and instrument

2.1 The instrument: GLORIA

GLORIA is part of the heritage of CRISTA-NF, which was a limb viewing airborne instrument with a vertical resolution of 200 – 400 m and two spectrometers with spectral resolution of $\approx 2\,\mathrm{cm}^{-1}$ and $\approx 1\,\mathrm{cm}^{-1}$, respectively. This instrument represented an important step stone toward future remote sensing limb instruments with even higher vertical and horizontal resolution. The GLORIA instrument and the data processing chain is described in previous studies, therefore the reader is referred to the works of Kleinert et al. (2014), Friedl-Vallon et al. (2014), Riese et al. (2014) and Ungermann et al. (2015) for a more detailed description. Here the main concepts are presented.

GLORIA is an infrared limb emission sounder that combines the Fourier-transform spectroscopy with a 2D infrared detector and measures radiances in the mid-infrared range (780 – 1400 cm^{-1}). It was designed with the purpose of providing information in the observational gap that comprises small-scale structures of less than 500 m of vertical extent and less than 100 km in the horizontal. With GLORIA, it is possible to retrieve the distribution of different trace gases and aerosols, reconstruct gravity waves and study clouds in the UTLS (e.g. Blank, 2013; Krisch et al., 2018; Höpfner et al., 2019). The high spatial resolution, $140 \times 140\,\mathrm{m}$ (horizontal sampling $\times$ vertical sampling) at a tangent point altitude of 10 km and observer altitude of 15 km, and the high precision sensors to obtain a good pointing accuracy, make GLORIA a perfect instrument for measuring optically and vertically thin cirrus. The instrument is typically configured to use 48×128 pixels of its 2D detector array. As the main focus of this study is the characterization of cirrus clouds close to the tropopause and thus the most important feature is the vertical resolution, we do not analyze each individual pixel, but the horizontally averaged spectrum of each line of the 2D array. The final result is one profile for each measured set of interferograms with 128 spectra. The amount of radiance that each pixel receives is determined by the point spread function (PSF). The shape of the PSF is approximated by an Airy-disk with an aperture of 2.01. This configuration has been computed from a theoretical set-up of the instrument and was validated by cloud top measurements.

GLORIA is typically configured to one of three measuring modes: one high spectral resolution mode called chemistry mode (CM) and two modes, premier and panorama modes (DM), focusing on dynamical effects in the atmosphere. During the premier and panorama mode, the instrument changes its viewing direction between 45° and 135° in steps of 4° and 2°, respectively, which gives the possibility of observing the same volume of air from different perspectives and thus allowing for tomographic studies. This capability of GLORIA is used for the reconstruction of gravity waves (Krisch et al., 2018) and clouds (Ungermann et al., 2020). Table 1 summarizes the most important technical characteristics of GLORIA. The data processing chain of GLORIA consists of three stages: the raw data processing (level 0), the processing into geolocated calibrated spectra

https://doi.org/10.5194/amt-2020-394
Preprint. Discussion started: 26 October 2020

Atmospheric Measurement Techniques Discussions

Table 1. Instrument specifications (Friedl-Vallon et al., 2014). Observer altitude of 15 km and tangent altitude of 10 km. *Ungermann (2020, in preparation)

Property	Value
Temporal sampling	2 s (≈0.5 km)/12.8 s (≈3.2 km) for DM/CM
Spectral coverage	780 – 1400 cm^{-1}
Spectral sampling	0.0625 cm^{-1} to 0.625 cm^{-1}
Detector array size	256 × 256 pixels
Used detector array size	48 × 128 pixels
Vertical sampling	0.031°, equal to 140 m
Horizontal sampling	0.031°, equal to 140 m
Vertical spatial coverage	-3.3° below horizon to 0.8° above horizon
Horizontal spatial coverage	1.5°(=48 × 0.031°) equal to 6.7 km
Yaw pointing range	45° to 135°
Pointing precision (vertical)	0.012°, equal to ≈50 m (1σ)
*Pointing accuracy	0.1°

(level 1) and the retrieval of geophysical quantities leveraging the fast radiative transfer model JURASSIC2 (section 2.4). This work uses level 1 and level 2 products.

2.2 The campaign: WISE

The data analyzed in this study was measured during the WISE (Wave-driven ISentropic Exchange) campaign. It took place in Shannon, Ireland (52.70°N, 8.86°W) in September and October of 2017. With a total of fifteen scientific flights (Fig. 1) covering the North Atlantic area, it aims to answer questions related to mixing, the role of Rossby wave breaking events in the transport of trace gases, such as water vapor, the formation of cirrus clouds and several other topics (Riese et al., 2017, last accessed: 13 August 2020). All the measurements were taken onboard the German research aircraft HALO (High Altitude and Long Range Research Aircraft), where GLORIA was placed in the belly-pod. HALO can fly to a maximum altitude of 15 km, which means that the vertical coverage of GLORIA observations during this campaign ranges from ∼15 km down to ∼5 km.

2.3 Meteorological dataset

We used the high resolution ERA5 data-set provided by the European Centre for Medium-Range Weather Forecasts (ECMWF). The reanalysis data are available at 31 km horizontal resolution at 137 levels from surface to 80 km (Hersbach et al., 2020). The ERA5 dataset provides hourly data for a large variety of meteorological and climate variables. To perform the comparison between model and measurements, the variables of interest were sampled according to the GLORIA measuring geometry, as shown in Fig. 2. This figure represents the limb geometry during one measurement. For every line-of-sight (LOS), every 30 km, the meteorological variables were computed from the corresponding parameters of the ERA5 data set, i.e. first thermal

https://doi.org/10.5194/amt-2020-394
Preprint. Discussion started: 26 October 2020

Atmospheric Measurement Techniques Discussions

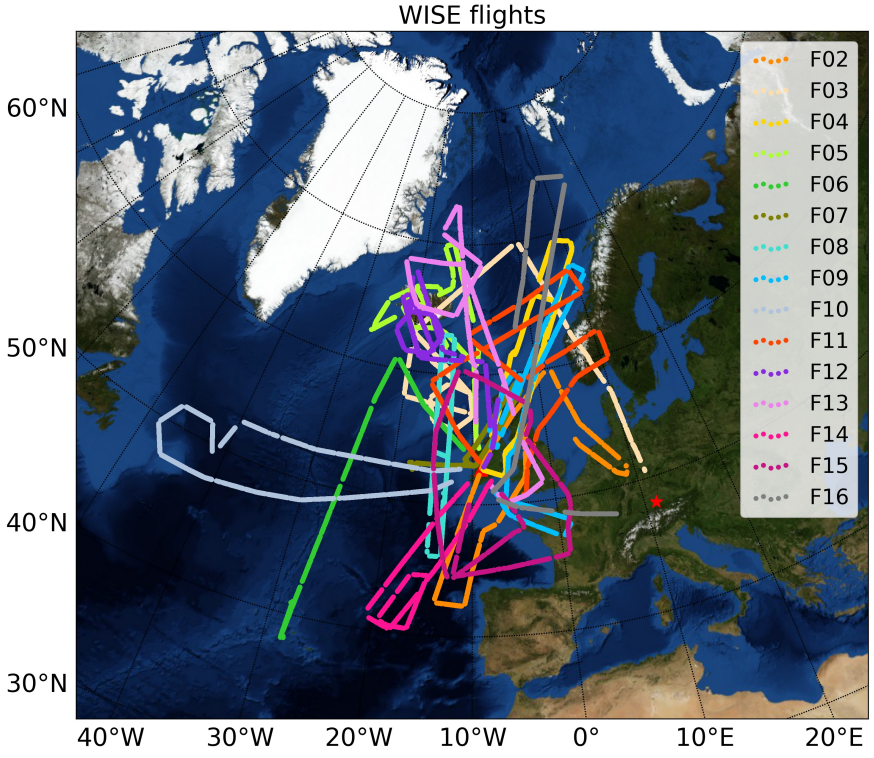

Figure 1. Overview of the 15 scientific flights of the WISE campaign. Color points correspond to the positions of HALO with GLORIA measuring. The red star indicates Oberpfaffenhofen, Germany and the red triangle Shannon, Ireland (NASA's Earth Observatory).

tropopause (TP), equivalent latitude and ice water content (IWC). As the signal is integrated along the LOS of the instrument, the same applies for the IWC, thus the final parameter used for the comparison is the limb ice water path (IWP), i.e. the IWC integrated along the LOS (Spang et al., 2015). In addition, we retrieved the potential vorticity (PV) and equivalent latitudes from the ECMWF data at the tangent point. The static stability (N^2) used to analyze the stability of the atmosphere was computed from GLORIA retrievals. The potential temperature product needed for the computation of N^2 was computed from pressure and temperature of the final data set, which contains the retrieval results and a priori information taken from ECMWF. The results are dominated by a priori in regions where no measurements are available, i.e., in or below thick clouds.

2.4 The model: JURASSIC2

The JUelich Rapid Spectral Simulation Code V2 (JURASSIC2) is a fast radiative transfer model developed at Forschungszentrum Jülich for analyzing the measurements of remote sensing instruments (Hoffmann, 2006). It combines a forward model with

https://doi.org/10.5194/amt-2020-394
Preprint. Discussion started: 26 October 2020

Atmospheric Measurement Techniques Discussions

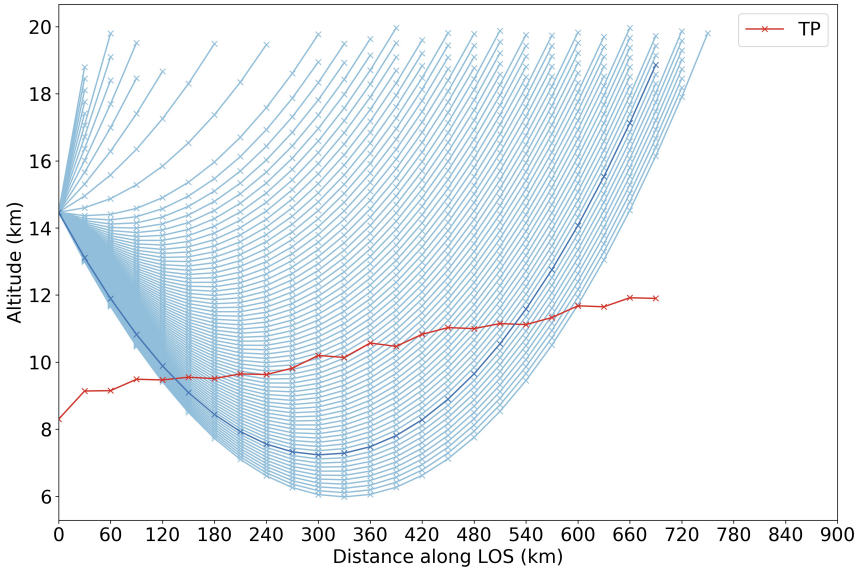

Figure 2. Example of the measuring geometry of GLORIA. The red line indicates the tropopause (TP) from ERA5 along the corresponding line-of-sight (LOS), in dark blue.

retrieval techniques and allows us to derive pressure, temperature and trace gas volume mixing ratios among others. JURASSIC2 solves the Schwarzschild Equation in the mid-infrared region using spectrally averaged radiances, the Curtis-Godson Approximation (CGA; Curtis, 1952; Godson, 1953) and Emissivity Growth Approximation (EGA; Weinreb and Neuendorffer, 1973; Gordley and Russell, 1981) in combination with emissivity look up tables (LUT) (Ungermann et al., 2011). The LUT are typically computed by the line-by-line Reference Forward Model (Dudhia, 2017).

JURASSIC2, together with the Juelich Tomographic Inversion Library (JUTIL), generates the level 2 products (temperature, trace gases, extinction coefficient). For a detailed description of this process the reader is referred to Ungermann et al. (2015). For this study, the level 2 product used is simply the extinction coefficient. An explanation of how it is retrieved is given in Sect. 3.2.

3 Cloud detection methods

To analyze the data, two methods to identify optically and vertically thin clouds at high altitudes were used, a cloud index and the extinction coefficient.

https://doi.org/10.5194/amt-2020-394
Preprint. Discussion started: 26 October 2020


Atmospheric Measurement Techniques Discussions

3.1 Cloud index

The cloud index (CI) was first introduced by Spang et al. (2001) and has been widely used in different studies for the analysis of clouds in the UTLS and polar stratospheric clouds observed by CRISTA and MIPAS (Sembhi et al., 2012; Spang et al., 2015, 2016). The CI is a dimensionless number defined as the ratio between the mean radiances of two microwindows:

$$\frac{I(788.2-796.2)\mathrm{cm}^{-1}}{I(832.4-834.4)\mathrm{cm}^{-1}} \tag{1}$$

The first spectral window is mainly dominated by emissions of a CO_2 Q-branch and the second is an atmospheric window region. The CI is affected by the water vapor continuum contribution to the atmospheric window at low altitudes and depends slightly on latitude and season (Sembhi et al., 2012). When clouds are present, the emission in both microwindow increases. However, the relative increase in the CO_2 Q-branch is smaller. As a result, the ratio decreases, therefore low values of CI indicate cloudy conditions. A $\sim 1.1 < \mathrm{CI} < 4$ indicates the presence of clouds (Spang et al., 2008, 2015).

3.2 Extinction coefficient retrieval

The extinction coefficient (from now on simply extinction) was retrieved with JURASSIC2. Although scattering by cloud particles has an impact on the measured radiance (Höpfner and Emde, 2005), we simulated the radiative transfer without scattering. As explained by Höpfner and Emde (2005) the difference between zero scattering and multiple scattering for a case that falls between the two cases presented in their study (ω_0 = 0.24 and ω_0 = 0.84), would be between 25-28 %. Additionally, we performed test runs with single scattering for two flights using the radiative transfer model JURASSIC2. The difference between the extinction neglecting scattering and the extinction including single scattering is 21 %, with 73 % as the percentile 95 and -86 % as the percentile 5 (results not shown). We considered that for our current purpose of obtaining macro-physical properties of cirrus clouds the non-scattering approach is sufficient.

Obtaining the extinction means solving an ill-posed inverse problem. In our inverse problem, there is a state vector $\boldsymbol{x}$ describing the state of the atmosphere (quantities to be retrieved), a measurement vector $\boldsymbol{y}$ with error $\boldsymbol{\epsilon}$, and a forward model $\boldsymbol{F}$ implementing the physics of the involved processes.

$$\boldsymbol{y} = \boldsymbol{F}(\boldsymbol{x}) - \boldsymbol{\epsilon} \tag{2}$$

For this work, $\boldsymbol{x}$ is the extinction and $\boldsymbol{y}$ is the radiance in the microwindow 832.4 – 834.4 cm^{-1}. This interval is the same one used for the CI.

The retrieval grid consists of a constant altitude grid with 81 levels ranging from 6 km to 16 km with a sampling distance of 0.125 km. The model includes corrections of the tangent altitudes due to the elevation angle offset and the refraction. Several tests comparing the radiance of a theoretical case of a cloud as a step function and the retrieved one were performed to determine the influence of the radiance of cloudy pixels on the pixels above (not shown), i.e. the effect of the PSF. The results show that the retrieved profiles are affected by Gibbs oscillations that cause ringing artifacts at the edges and an overshoot of ≈10 % is found (i.e. radiance value larger than the maximum of the step function). These effects can cause an error in the determination

https://doi.org/10.5194/amt-2020-394
Preprint. Discussion started: 26 October 2020


Atmospheric Measurement Techniques Discussions

of the cloud top height of one grid point ($\pm$ 125 m). These oscillations could also affect the determination of the cloud bottom, creating a false detection of a thin layer (1 – 2 pixels) above a thick cloud in $\approx 1\,\%$ of all the cloudy profiles. The leading error term in the determination of the cloud top altitude is the pointing knowledge along the LOS. This error is about a tenth of a degree, which has been validated by measurements of the Moon during several flights (Ungermann, 2020, in preparation).

The range of retrievable extinction values for clouds is from about $2\times10^{-4}\,\mathrm{km}^{-1}$ to $4\times10^{-2}\,\mathrm{km}^{-1}$ and allows for the detection of optically thin cirrus, one of the objectives of this study. The upper limit is determined by the optical thick conditions in the limb direction and the lower limit by background aerosol and calibration uncertainties.

We sampled the CI on the extinction retrieval grid to allow for a comparison of both methods (Fig. 3). The radiative transfer model assumes for practical reasons a horizontal homogeneous atmosphere. As such, it assumes that simulated measurement rays diving below a cloud layer passes through the cloud twice, whereas in the actual situation it may 'miss' the cloud on both occasions; if this occurs, the retrieval assigns nonphysical low extinction values close to 0 to those regions (Fig. 3a, e.g. at 11:29 UTC, 11 – 12 km). Above the clouds, the low extinction is due to the second order regularization that smooths the profiles and causes Gibbs oscillations in the extinction profile at strong value changes. For the CI cross-section (Fig. 3b), depending on the altitude, different CI threshold values indicate the presence of clouds. A detailed explanation about the detection threshold is found in Sect. 3.3.

3.3 Detection threshold for CI and extinction

To identify clouds in the measurements, we defined the detection thresholds for CI and extinction. First, we define the criteria for clear sky regions. As a first approximation of clear sky conditions, profiles with CI always greater than 2 and extinction always less than $10^{-3}\,\mathrm{km}^{-1}$ were selected. From this first coarse pre-selection, the vertical extinction gradient (Fig. 4) was computed to have an automated method that is more sensitive to optically thin clouds. If this gradient has a small variability, that means there are no elements that cause a sudden increase in the extinction. Clear sky profiles were defined to be those with an extinction gradient lower than a threshold defined as the median extinction gradient of the pre-selected profiles of all flights together plus 5σ. A value of 5σ was chosen after a visual fit to the gradient to reduce the number of false detections to a minimum. It is possible that the aircraft flies inside a cloud, which causes the vertical gradient of the extinction to be approximately constant and thus considered as clear sky. To exclude these cases, the condition that the CI must always be greater than 2 was added. Below 8 km the extinction gradient increases, which indicates the influence of the water vapor continuum at low altitudes (Fig. 4). Therefore, the analysis was limited to the range from 8 km to the aircraft altitude. For all the clear sky profiles, PDFs of CI and extinction were calculated and normalized for each altitude bin. Using the PDF for guidance, a threshold for each parameter is defined. The extinction coefficient threshold (k_{thres}) was defined as the median of the extinction plus 5σ. This threshold is sensitive to structures with very low extinction, down to $2\times10^{-4}\,\mathrm{km}^{-1}$ for a tangent point between $\sim$11.5 km and 15 km. This value is similar to the one provided by Sembhi et al. (2012) for MIPAS, with an extinction detection limit above 13 km of $10^{-4}\,\mathrm{km}^{-1}$ and to the findings of Griessbach et al. (2020). The CI threshold ($\mathrm{CI}_{\mathrm{thres}}$) is the percentile 1 (%) shifted by 0.3 (CI). Above 12 km we applied a constant CI-value of 5 because there, the low number of counts shifts the threshold towards too high values of CI. This value, as well as the threshold for lower altitudes, agrees

https://doi.org/10.5194/amt-2020-394
Preprint. Discussion started: 26 October 2020

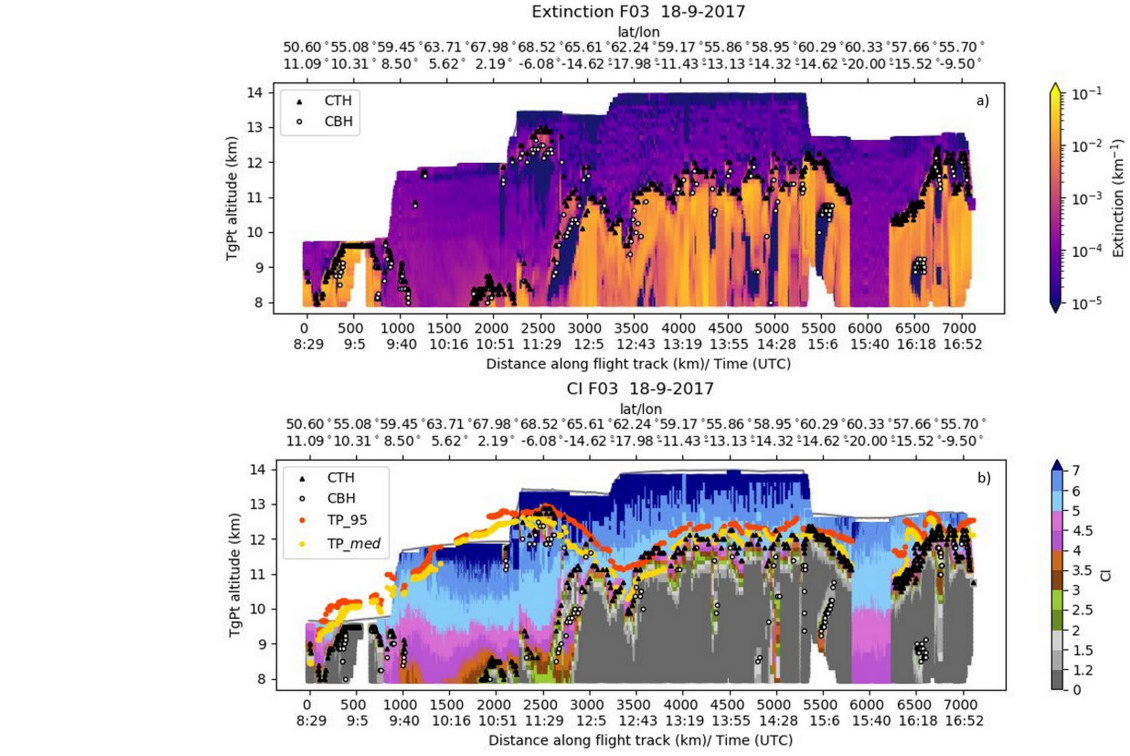

Figure 3. Cross-sections of extinction (a) and cloud index (b) for flight 3 of the WISE campaign. The results are restricted to levels below flight path. (a) Color code for extinction in km^{-1}. Orange-pink colors indicate the presence of clouds; (b) color code for CI. Depending on the altitude, CI values below 2 to 5 (colors from grey to pink) indicate the presence of clouds. Median tropopause (TP_{med}) and the percentile 95 of the tropopause (TP_{95}) are represented with orange and yellow circles, respectively. Cloud top height (CTH) and cloud bottom height (CBH) are represented with a black triangle and with a white circle, respectively. The altitude of the tangent points (TgPt) is the y axis. The white areas in both cross-sections correspond to a first filtering of optically thicker regions (CI < 2).

with the one defined by Sembhi et al. (2012) for northern mid-latitudes and Spang et al. (2012) for the MIPAS instrument. The threshold lines separate the clear air and cloudy cluster from each other, following the vertical gradient of the clear air cluster (Fig. 5).

3.4 Definition of the macro-physical characteristics

Here, we define the macro-physical characteristics of the detected cirrus clouds that are presented in Sect. 4: cloud top height (CTH), cloud bottom height (CBH) and vertical extent. In the limb geometry, the position of the cloud along the LOS is not exactly known. For analyzing the data, the clouds were referred to the tangent point, i.e., the point of the LOS closest to the Earth's surface and the corresponding tangent height layer. Using this definition of the position of the cloud, the CTH was defined as the first point in which the extinction (or CI) has a value equal to or larger than the k_{thres} (or less than or equal to

https://doi.org/10.5194/amt-2020-394
Preprint. Discussion started: 26 October 2020

Atmospheric Measurement Techniques Discussions

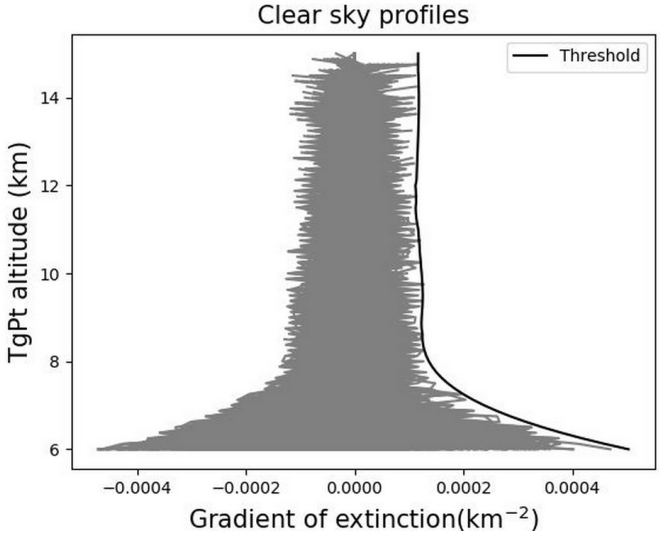

Figure 4. Clear sky profiles of the vertical gradient of the extinction coefficient for all flights together. In black, the threshold defined as the median of the extinction gradient plus 5σ. Altitude of the tangent points (TgPt) in the y axis.

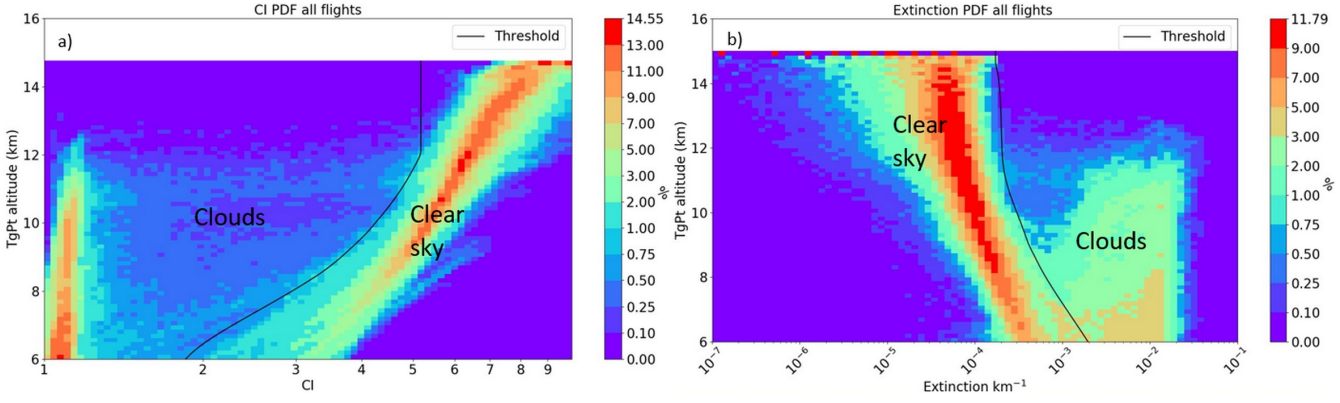

Figure 5. PDF for CI and extinction for all flights including all profiles. The bins are normalized by altitude. In black the threshold for differentiating cloudy conditions from clear sky. For (a) clouds correspond to small values of CI, i.e, the left side of the CI_{thres}. For (b) clouds correspond to high extinction values, i.e., to the right side of the k_{thres}. The altitude of the tangent points (TgPt) is the y axis. The total number of analyzed profiles is 13539.

the CI_{thres}). For the analysis, we assumed a homogeneous cloud layer, which may underestimate the real extinction. This could cause an underestimation of the CTH for some cases, in which the cloud is on the ray path far from the tangent point location (Kent et al., 1997). All the CTHs belong to the first cloud detected, i.e., the analysis did not include multi-layer clouds (two or more clouds with a clear separation in between). The CBH of a cloud using the extinction method is the altitude of the first point with an extinction smaller than the k_{thres}; this ensures the identification of an altitude at or below the true cloud bottom.

https://doi.org/10.5194/amt-2020-394
Preprint. Discussion started: 26 October 2020

Atmospheric Measurement Techniques Discussions

For the CI method, the CBH was computed using the minimum of the CI gradient of the profile (Kalicinsky et al., 2020). CBH could only be reliably determined for optically thin clouds. For optically thick conditions, the CI profiles saturate and the extinction profiles decrease in an unrealistic manner. Optically thick profiles are characterized by CI-values lower than 1.2 from an altitude *h* down to the lowest altitude (Spang et al., 2015, 2016). Thin profiles are those for which it was possible to define a CBH. Figure 6 shows an example of a saturated CI profile and a profile for a cloud layer. It is possible to observe how the saturated CI profile reaches saturation after CI = 1.2. The last macro-physical characteristic that was analyzed is the vertical extent, defined as the CTH – CBH.

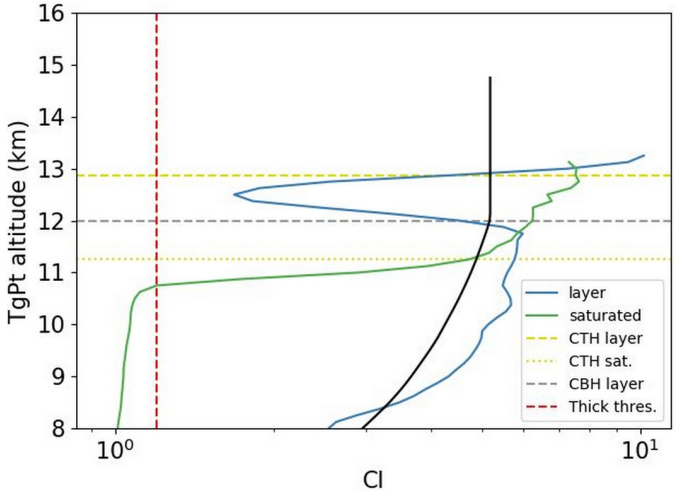

Figure 6. CI profile for a cloud layer (blue) and an optically thick case (green) that saturates. The horizontal yellow lines indicate the cloud top height (CTH) for the layer (dashed line) and the thick case (dashed point line). The horizontal dashed line in grey is the cloud bottom height (CBH) of the cirrus layer. The red vertical line corresponds to CI = 1.2 i.e. optically thick cases. In black, the CI threshold. The altitude of the tangent points (TgPt) is the y axis.

3.5 Differentiation between clouds and aerosol

Enhanced aerosol number densities can also affect the CI values and cause false cloud detection. To investigate if the presence of aerosol particles influenced the results, methods described by Griessbach et al. (2014) and Griessbach et al. (2016) were applied. These methods use the different spectral slopes of ice and aerosols, such as volcanic ash or sulfuric acid, in five wavelength regions to establish thresholds that differentiate them. The results (not shown), indicated very little influence of these aerosols in our measurements.

https://doi.org/10.5194/amt-2020-394
Preprint. Discussion started: 26 October 2020


Atmospheric Measurement Techniques Discussions

4 Results

4.1 Analysis: cloud top height and cloud bottom height

During the WISE campaign, 61% of all observed profiles show CTHs using the extinction method and 59% for the CI. These values are comparable to the climatology presented in Goldfarb et al. (2001) for lidar observations, with a cirrus occurrence frequency of 60% for fall. However, 60% is considerably larger than the ≈17% reported by Sassen et al. (2008) for CALIPSO measurements and the International Satellite Cloud Climatology Project (ISCCP) for mid-latitudes. It is rather unlikely that this difference is related only to the disparate observational periods. We rather explain it by the differences in cirrus cloud selection criteria of the studies.

The extinction method and the CI method show good agreement in the determination of the CTHs, presenting a similar distribution (Fig. 7 a and b). The CTHs between 8 and 10 km present equivalent latitudes that spread from tropical to polar regions, having a slightly higher frequency at the polar latitudes. For CTHs between 10 km and about 12.5 km the air masses have an equivalent latitude typical of mid-latitudes, whereas the highest CTHs, above about 12.5 km are almost subtropical. The main difference between both methods is the slightly higher (1 – 2 pixels) CTHs of the CI method.

Considering all observed profiles about 39 % are optically thick using the extinction and 41 % the CI method. The maximum extinction detected for thin clouds in which a CBH was possible to determine is $4 \times 10^{-2}\,\mathrm{km}^{-1}$.

The distribution of the vertical extent of clouds is presented in Fig. 8. The extinction method results in a higher amount of vertically thin clouds than the CI method, due to the slightly higher CBHs of the extinction method (Ungermann et al., 2020). For both methods, a large fraction of the optically thin cirrus clouds have a vertical extent smaller than 1.5 km (31 % of the clouds detected with the extinction method and 20 % of the clouds detected with the CI method). These results are qualitatively similar to the findings of Noël and Haeffelin (2007). They show that between May and November the vertical extent distribution of the observed clouds is biased towards values between 0 and 1.5 km. Our results are also in agreement with the mean layer thickness of 1.4 km computed by Goldfarb et al. (2001).

4.2 Cloud top position with respect to the tropopause

The occurrence frequency of cirrus clouds above the tropopause remains a matter of debate. The vertical resolution of the underlying temperature profile of the meteorological analysis for the tropopause computation is a key point for respective analyses. As discussed in Pan and Munchak (2011) different definitions of the tropopause can lead to different results. For this study, the first thermal tropopause altitude was computed from ERA5 data. The LOS of GLORIA typically extends several hundreds of kilometers sampling air masses that can be heterogeneous. Consequently, the tropopause is usually not constant along the LOS (Fig. 2). Two methods were applied for representative tropopause definition for the air mass sensed by the instrument: a) the median of the tropopause along the corresponding LOS of the CTH and b) the 95 % percentile. All extinction and CI cross-sections of the WISE campaign with CTHs, CBHs, median tropopause (TP_{med}) and 95 % percentile (TP_{95}) can be found in the supplement. Figure 3 illustrates the case of a flight with both homogeneous and heterogeneous air masses. E.g. the air mass at 16:18 UTC is homogeneous and TP_{med} and TP_{95} are close to each other (less than 125 m apart). At 11:29 UTC,

https://doi.org/10.5194/amt-2020-394
Preprint. Discussion started: 26 October 2020

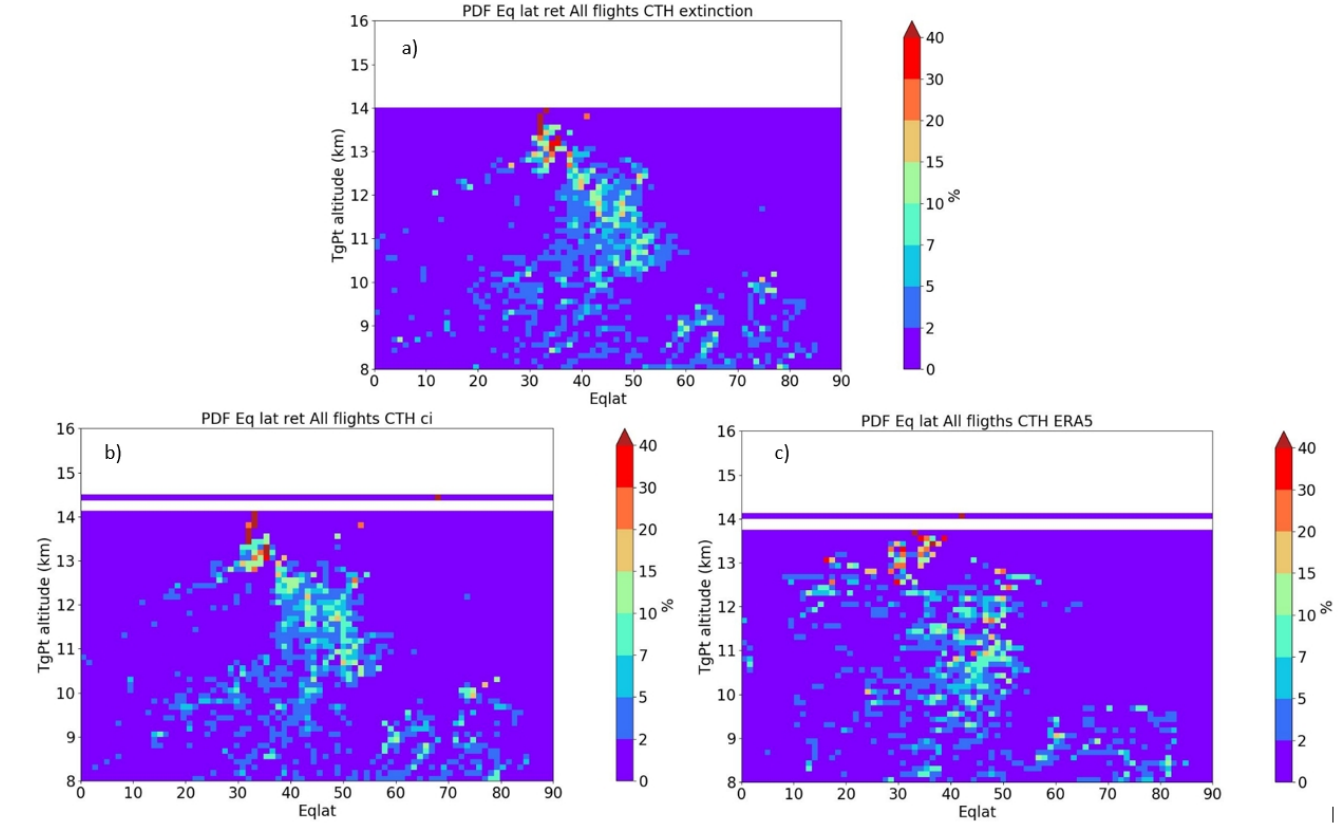

Figure 7. PDFs of equivalent latitude (Eqlat) normalized for each altitude bin for (a) CTH detected with the extinction, (b) CTH detected with the CI and (c) CTH from ERA5. The altitude of the tangent points (TgPt) is the y axis.

there are heterogeneous air masses with TP_{med} and TP_{95} separated (three times the distance of the previous example), which affects the statistics of CTHs above the tropopause, since the CTH is above or below the tropopause depending on the chosen tropopause altitude.

For the extinction method, the frequency of occurrence of CTHs above the TP_{med} is 24 % of the total number of observations, whereas for the CI method the ratio is 27 % (Fig. 9b). The ≈3 % difference is due to the CI detecting CTHs slightly higher than the extinction method. When considering TP_{95}, the percentages decrease to 13 % and 16 % respectively as it uses a more conservative criterion. This gives confidence to conclude that CTHs above the lapse rate tropopause were detected, even when considering the error in the CTH determination, which is in the order of ±125 m. Figure 10 shows the distribution of all CTHs and CTHs above TP_{med} for the extinction method. About 6 % of all profiles show for both methods CTHs above the TP_{med} and are classified as optically thin. The ratio of clouds with both CTH and CBH above the TP_{med} is 2 % for the extinction method and 1 % for the CI method. When considering the TP_{95}, both percentages decrease but still detect CBHs above the TP. The presence of complete layers above the tropopause is inconclusive, as these CTHs and CBHs are in general just one altitude

https://doi.org/10.5194/amt-2020-394
Preprint. Discussion started: 26 October 2020

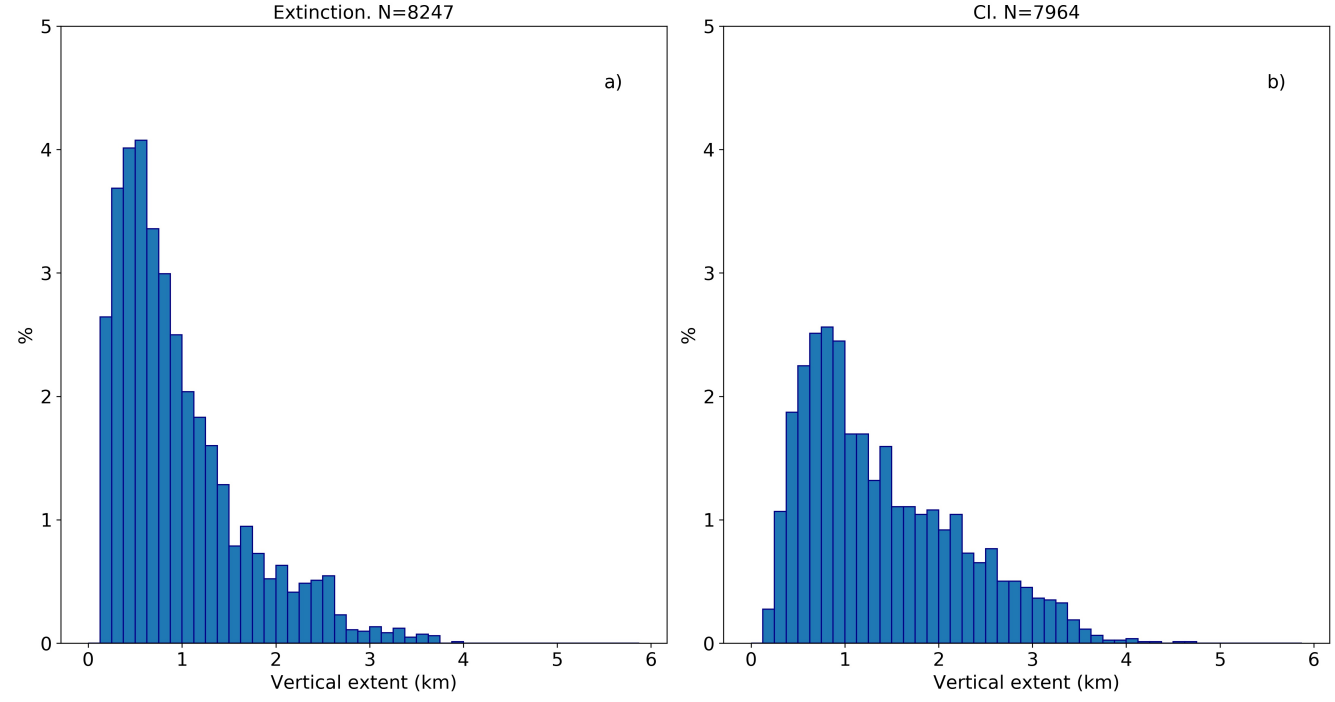

Figure 8. Distribution of the vertical extent of cirrus clouds for all flights for (a) the extinction method and (b) the CI method. The percentage is given in relation to the total number of CTHs (N) detected for each method.

bin apart and the CBH is only one or two altitude bins above the tropopause, which is within the uncertainties of the CBH. In Sect. 4.4, a potential case of a cloud layer above the tropopause is discussed in more detail. Our results (summarized in Table 2) agree with previous studies that claim the detection of CTHs above the tropopause for mid-latitudes. Goldfarb et al. (2001) used lidar ground based instruments and found 5 % of CTHs at least 1 km above the tropopause, and approximately 15 % above 0.5 km. Spang et al. (2015) analyzed CRISTA data (Spang et al., 2015) and concluded with a frequency of occurrence of 5 % of all observations and Zou et al. (2020) obtained 2 % for CALIPSO data and 4 – 5 % for MIPAS data. The analyses of Spang et al. (2015) and Zou et al. (2020) used the criterion of the cirrus CTH being 0.5 km above the tropopause derived from ERA-Interim. Using the same criterion, the frequency of occurrence is 4 % for CTHs above the TP_{med} for the extinction method and 7 % for the CI method. These values are comparable to the ones of the literature. However, as we used ERA5 data, which has a better vertical resolution than ERA-Interim, the equivalent criterion would be 0.25 km above the tropopause. In this case, the frequency of occurrence increases to 13 % above the TP_{med} for the extinction method and to 17 % for the CI method. We explain the differences in the frequency of occurrence by different periods being compared, the sensitivity and vertical resolution of the instruments, the uncertainty of the meteorological data used to estimate the tropopause height and the definition of stratospheric cirrus used in each study.

https://doi.org/10.5194/amt-2020-394
Preprint. Discussion started: 26 October 2020

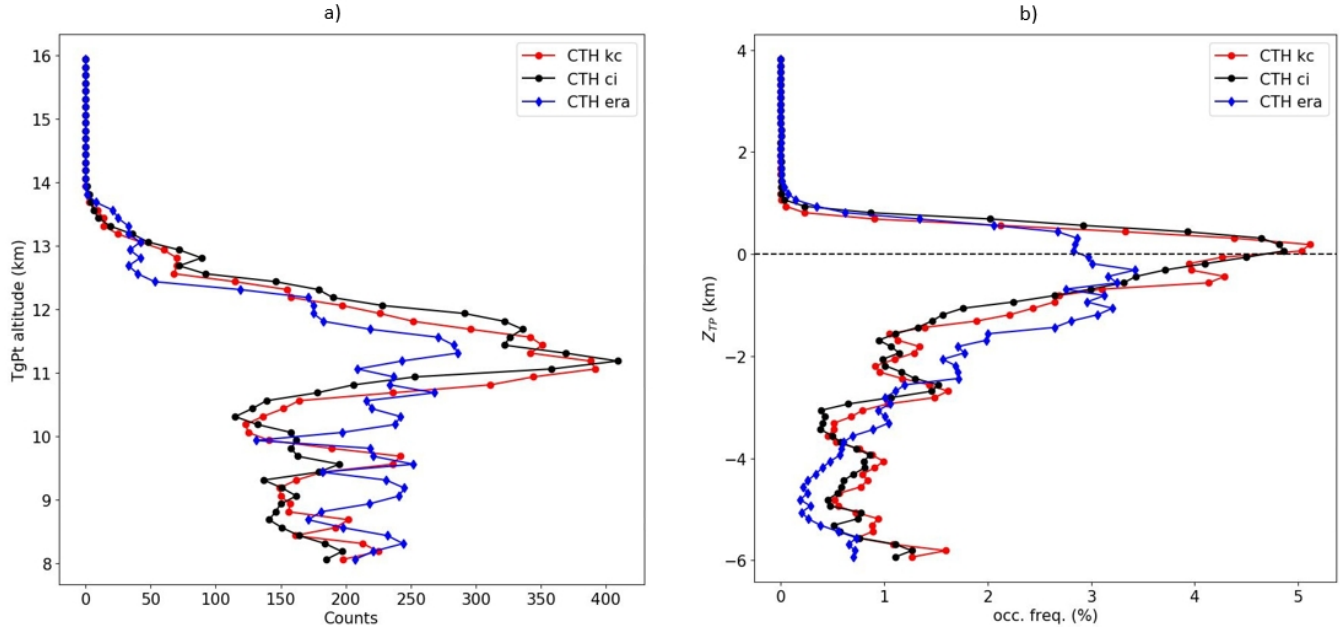

Figure 9. (a) Number of cloud top heights (CTH) per altitude bin for the extinction method (*kc*) in red, the CI method (black) and ERA5 (blue). The altitude of the tangent points (TgPt) is the y axis. (b) The same as a) but using as coordinates the distance of the CTHs to the tropopause in km (Z_{TP}). The used tropopause is the median tropopause (TP_{med}). The three profiles have been smoothed with a three points running mean.

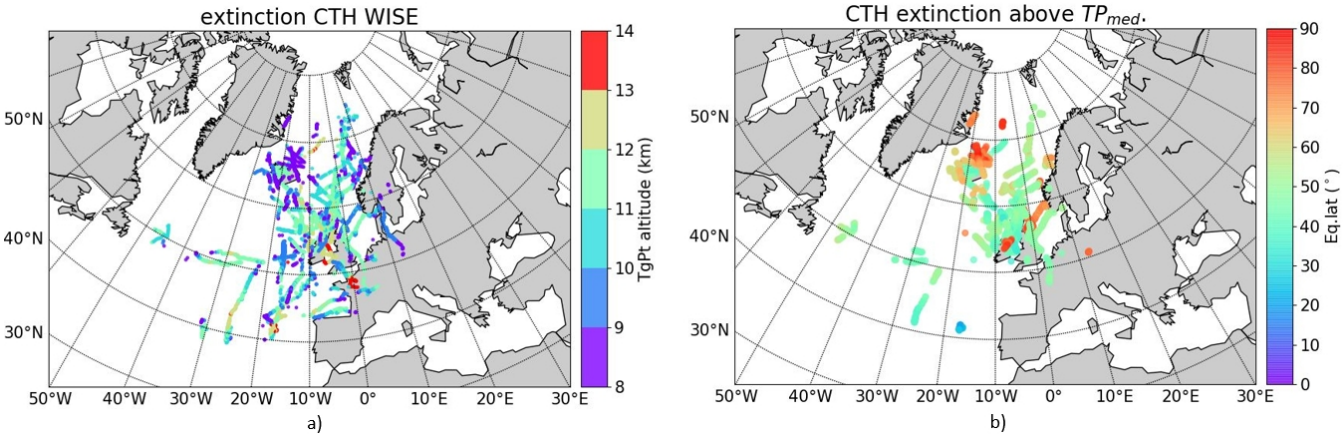

Figure 10. Distribution for (a) all cloud top heights (CTHs) for extinction with color code as the tangent point altitude in km (TgPt) and (b) CTHs for extinction above the median tropopause (TP_{med}) with color code equivalent latitude (Eqlat).

https://doi.org/10.5194/amt-2020-394
Preprint. Discussion started: 26 October 2020


Atmospheric Measurement Techniques Discussions

Table 2. Percentage with respect to all retrieved profiles of cloud top heights (CTHs) and cloud bottom heights (CBHs) detected above the median tropopause (TP_{med}) and the percentile 95 of the tropopause (TP_{95}) for both detection methods.

	TP_{med}		TP_{95}	
	CI	ext	CI	ext
CTH all	27	24	16	13
CTH thin	7	7	5	4
CTH and CBH	1	2	1	1

4.3 Comparison with ERA5

We compared our CTH detections with the ERA5 data-set by applying the observation geometry of GLORIA. As explained in Sect. 2.3, one of the variables sampled following the viewing geometry of the GLORIA instrument is the IWC for ERA5, which when integrated along the LOS results in the limb IWP. Spang et al. (2012) showed that CI and the limb IWP divided by the effective radius of the particles size distribution are very well related to each other. This is caused by the fact that for large particles (with respect to the wavelength) the observed cloud radiances are determined by the integrated surface area along the LOS, in contrast to the volume density for small particles. We defined a CTH for the ERA5-based data-set to each tangent point with IWP > 0.

Figure 7c shows a similar distribution of CTHs in ERA5 data as the one derived from the measurements. The fraction of CTHs detected in ERA5 is about 59 % of all profiles, the same as the one of the CI method (59 %) and only slightly lower than the fraction for the extinction method (61 %). Figure 9a shows that between 8 and 11 km altitude, ERA5 indicates more frequent CTHs than the observations. This could be related to not considering multi-layer clouds in the detection algorithm, which would mean increase the number of CTHs observed between 8 and 11 km. The instrument is sensitive to higher and thinner cirrus clouds than the clouds assimilated by ERA5. Consequently, high CTHs detected by GLORIA will hide lower and thicker CTHs in the ERA5-based data-set. When changing to a coordinate system with respect to the TP_{med} (Fig. 9b), the distribution of all CTHs is similar beyond 0.5 km distance from the TP_{med}. Between -0.5 km and 0.5 km, there are more CTHs measured than for ERA5. Considering all occurrences above the TP_{med}, the observations detect about 50 % more than ERA5 data-set. This result indicates limitation in the cloud scheme used in the assimilation system of ERA5 for these optically thin clouds close to the tropopause.

4.4 Example of cirrus above the tropopause

In Sect. 4.2 the presence of complete layers above the tropopause was suggested, i.e., both CTH and CBH are found above the tropopause. As a case study, an observation made during flight 16 on the 21st of October was analyzed in more detail. Figure 11 shows a zoomed area of the cross-section of the flight. Only cloudy points are colored for both the extinction method and CI. The corresponding TP_{med} and TP_{95} have close values, indicating that the sampled air masses are homogeneous with respect to the temperature structure around the tropopause. Both methods identify cirrus cloud at 72.59° N and 69.38° N with

https://doi.org/10.5194/amt-2020-394
Preprint. Discussion started: 26 October 2020

Atmospheric Measurement Techniques Discussions

CTHs well above the tropopause (∼0.5 to 1 km for the first cirrus cloud and ∼0.5 km for the second). The CBH is slightly higher for the extinction method and above the tropopause, but still within the detection error, therefore, no affirmation of it being undoubtedly above the tropopause is made. In the location of the second cirrus there is a second tropopause at ∼18 km. Therefore, the CTH of this cirrus is in between tropopauses. Both clouds are optically thin, with an extinction between 3×10^{-4} and $5 \times 10^{-3}\,\mathrm{km}^{-1}$. The meteorological situation is characterized by a weak low pressure system on the surface close to Iceland, with an occluded front. The clouds are located in an area where the wind at 200 hPa changes from southwest to west to northwest with velocities between 20 – 28 $\mathrm{km\,h}^{-1}$. The air mass in both clouds have mid-latitude characteristics, with an equivalent latitude of approximately 51° N. The cloud at 72.59° N is in an area where the PV varies from 2.4 to 6 PVU and is in a stable region with N^2 between 1.6 and $5.2 \times 10^{-4}\,\mathrm{s}^{-2}$. These values of PV and N^2 indicate the transition region between troposphere and stratosphere (Kunz et al., 2009, 2011). The cloud at 69.38° N has PV values characteristic of stratospheric air masses, between 3.7 and 5.7 PVU and large static stability, $5.6 < N^2 < 7.1 \times 10^{-4}\,\mathrm{s}^{-2}$. Values of N^2 close to $7 \times 10^{-4}\,\mathrm{s}^{-2}$ are an indication of mixed sub-tropical and mid-latitudinal air masses (Kunz et al., 2009).

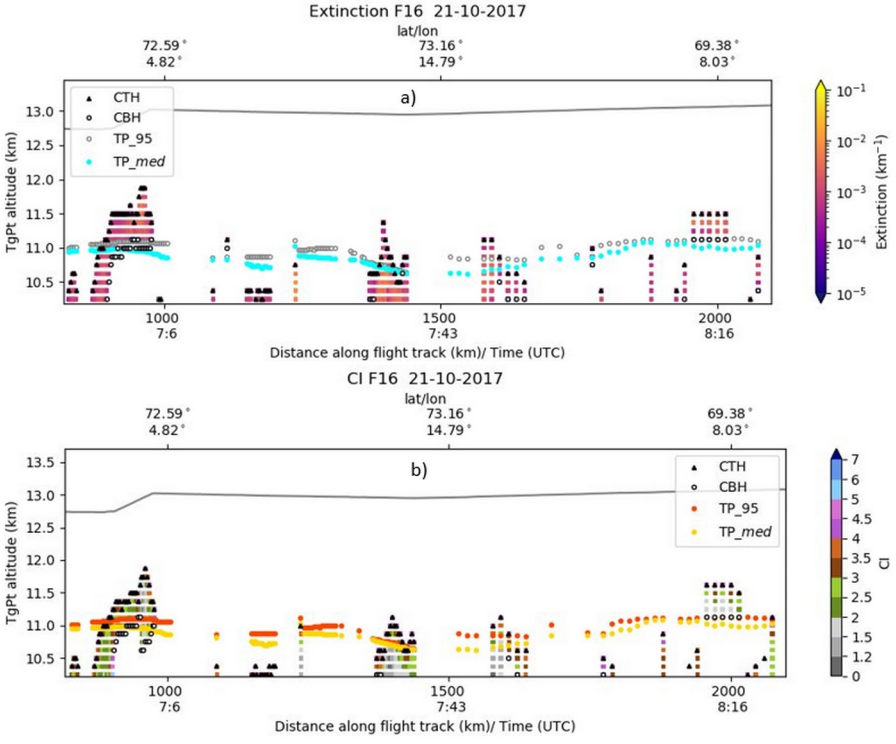

Figure 11. Zoomed area of the cross-section of flight 16 on the 21st of October 2017 focusing on two examples of thin cirrus above the tropopause. (a) Extinction coefficient color scale. Median tropopause (TP_{med}) and the percentile 95 of the tropopause (TP_{95}) are indicated with blue dots and grey dots, respectively. (b) Cloud index color scale. Median tropopause (TP_{med}) and the percentile 95 of the tropopause (TP_{95}) are indicated with yellow dots and orange dots, respectively. Black triangles indicate the CTHs and the white circles the CBHs. The altitude of the tangent points (TgPt) is the y axis.

https://doi.org/10.5194/amt-2020-394
Preprint. Discussion started: 26 October 2020


Atmospheric Measurement Techniques Discussions

5 Conclusions

In this study, we analyzed cirrus cloud observations taken with the limb sounder GLORIA on board of the research aircraft HALO during the WISE campaign. We used two methods for cloud identification, the cloud index and the derived extinction coefficient. The analysis focused on high cirrus clouds close to the tropopause and did not include multi-layer clouds. The extinction method indicated very thin clouds with an extinction of $2 \times 10^{-4}\,\mathrm{km}^{-1}$. Both methods are in good agreement, having similar frequencies of occurrence and similar CTHs. The main differences are the slightly higher CTHs of the CI method and the higher CBHs from the extinction method. For studying the presence of cloud tops above the tropopause we used two approaches. First, we calculated the median tropopause from ERA5 along the LOS of the GLORIA instrument and second, we used the more conservative 95th percentile. We considered similar tropopauses as an indication of homogeneous air masses. The frequency of occurrence above the tropopause varied from 27 % to 16 % for the CI and from 24 % to 13 % for the extinction method, where the difference between both approaches were due to LOS scenes with heterogeneous tropopause heights. Our results support the higher occurrence frequencies reported in literature (Goldfarb et al., 2001; Spang et al., 2015; Zou et al., 2020) in contrast to lower values derived from CALIPSO (Pan and Munchak, 2011; Zou et al., 2020) at mid-latitudes. Using the same criterion as in Spang et al. (2015); Zou et al. (2020), i.e. 0.5 km above the tropopause, the frequency of occurrence is 4 % – 7 %. However, as the ERA5 data-set presents a higher vertical resolution, when analyzing the frequency of occurrence 0.250 km above the tropopause, the value increases to 13-17 %. This means, that when the uncertainty of the tropopause estimate and the measurements is smaller, the stratospheric cirrus cloud occurrence frequencies are even higher. 1.5 km below the tropopause both identification methods present good agreement with the clouds indicated by the ERA5 data-set, when taken the observation geometry of GLORIA into account. However, the observed occurrence of cloud tops close to and above the tropopause is about 50 % higher than indicated by ERA5. We found CBHs above the tropopause, but they were within the uncertainties. Consequently, the GLORIA WISE campaign data cannot confirm the presence of unattached cirrus layers above the first thermal tropopause, but can confirm the presence of cirrus clouds at the tropopause with CTHs penetrating well into the lower stratosphere.

Data availability. The retrievals can be requested from the author.

Competing interests. The authors declare that they have no conflict of interests.

Acknowledgements. The authors are grateful to the ECMWF for providing operational analysis and forecast as well as reanalysis data. The authors acknowledge funding from the DFG, in the *Cirrus clouds in the extra-tropical tropopause and lowermost stratosphere region (CiTroS) project*, project number SP 969/1-1, part of the HALO Priority Program SPP 1294. Special thanks to the GLORIA team, including the

https://doi.org/10.5194/amt-2020-394
Preprint. Discussion started: 26 October 2020

Atmospheric Measurement Techniques Discussions

technology institutes ZEA-1 and ZEA-2 at Forschungszentrum Jülich and the Institute for Data Processing and Electronics at the Karlsruhe Institute of Technology. The authors also thank the WISE team, DLR-FX and the pilots.

https://doi.org/10.5194/amt-2020-394
Preprint. Discussion started: 26 October 2020

Atmospheric Measurement Techniques Discussions

References

Blank, J.: Tomographic retrieval of atmospheric trace gases observed by GLORIA, Ph.D thesis, Bergische Universität Wuppertal, Germany, https://juser.fz-juelich.de/record/150342, 2013.

Curtis, A. R.: Discussion of 'A statistical model for water vapour absorption' by R. M. Goody, Quart. J. Roy. Meteorol. Soc., 78, 638–640, 1952.

Dessler, A. E.: Clouds and water vapor in the Northern Hemisphere summertime stratosphere, J. Geophys. Res., 114, D00H09, https://doi.org/10.1029/2009JD012075, 2009.

Dudhia, A.: The Reference Forward Model (RFM), J. Quant. Spectrosc. Radiat. Transfer, 186, 243–253, https://doi.org/http://dx.doi.org/10.1016/j.jqsrt.2016.06.018, 2017.

Friedl-Vallon, F., Gulde, T., Hase, F., Kleinert, A., Kulessa, T., Maucher, G., Neubert, T., Olschewski, F., Piesch, C., Preusse, P., Rongen, H., Sartorius, C., Schneider, H., Schoenfeld, A., Tan, V., Bayer, N., Blank, J., Dapp, R., Ebersoldt, A., Fischer, H., Graf, F., Guggenmoser, T., Hoepfner, M., Kaufmann, M., Kretschmer, E., Latzko, T., Nordmeyer, H., Oelhaf, H., Orphal, J., Riese, M., Schardt, G., Schillings, J., Sha, M. K., Suminska-Ebersoldt, O., and Ungermann, J.: Instrument concept of the imaging Fourier transform spectrometer GLORIA, Atmos. Meas. Tech., 7, 3565–3577, https://doi.org/10.5194/amt-7-3565-2014, 2014.

Fusina, F., Spichtinger, P., and Lohmann, U.: Impact of ice supersaturated regions and thin cirrus on radiation in the midlatitudes, J. Geophys. Res., 112, D24S14, https://doi.org/10.1029/2007JD008449, 2007.

Godson, W. L.: The evaluation of infra-red radiative fluxes due to atmospheric water vapour, Quart. J. Roy. Meteorol. Soc., 79, 367–379, 1953.

Goldfarb, L., Keckhut, P., Chanin, M.-L., and Hauchecorne, A.: Cirrus climatological results from lidar measurements at OHP (44°N, 6°E), Geophys. Res. Lett., 28, 1687–1690, https://doi.org/10.1029/2000GL012701, 2001.

Gordley, L. L. and Russell, J. M.: Rapid inversion of limb radiance data using an emissivity growth approximation, Appl. Optics, 20, 807–813, 1981.

Griessbach, S., Hoffmann, L., Spang, R., and Riese, M.: Volcanic ash detection with infrared limb sounding: MIPAS observations and radiative transfer simulations, Atmos. Meas. Tech., 7, 1487–1507, https://doi.org/10.5194/amt-7-1487-214, 2014.

Griessbach, S., Hoffmann, L., Spang, R., von Hobe, M., Müller, R., and Riese, M.: Infrared limb emission measurements of aerosol in the troposphere and stratosphere, Atmos. Meas. Tech., 9, 4399–4423, https://doi.org/10.5194/amt-9-4399-2016, 2016.

Griessbach, S., Hoffmann, L., Spang, R., Achtert, P., von Hobe, M., Mateshvili, N., Müller, R., Riese, M., Rolf, C., Seifert, P., and Vernier, J.-P.: Aerosol and cloud top height information of Envisat MIPAS measurements, Atmos. Meas. Tech., 13, 1243–1271, https://doi.org/10.5194/amt-13-1243-2020, 2020.

Hersbach, H., Bell, B., Berrisford, P., Hirahara, S., Horányi, A., Muñoz-Sabater, J., Nicolas, J., Peubey, C., Radu, R., Schepers, D., Simmons, A., Soci, C., Abdalla, S., Abellan, X., Balsamo, G., Bechtold, P., Biavati, G., Bidlot, J., Bonavita, M., De Chiara, G., Dahlgren, P., Dee, D., Diamantakis, M., Dragani, R., Flemming, J., Forbes, R., Fuentes, M., Geer, A., Haimberger, L., Healy, S., Hogan, R. J., Hólm, E., Janisková, M., Keeley, S., Laloyaux, P., Lopez, P., Lupu, C., Radnoti, G., de Rosnay, P., Rozum, I., Vamborg, F., Villaume, S., and Thépaut, J.-N.: The ERA5 global reanalysis, Quart. J. Roy. Meteorol. Soc., 146, 1999–2049, https://doi.org/10.1002/qj.3803, 2020.

Hoffmann, L.: Schnelle Spurengasretrieval für das Satellitenexperiment Envisat MIPAS, Ph.D thesis, Bergische Universität Wuppertal, Germany, ISSN 0944-2952, 2006.

https://doi.org/10.5194/amt-2020-394
Preprint. Discussion started: 26 October 2020

Höpfner, M. and Emde, C.: Comparison of single and multiple scattering approaches for the simulation of limb-emission observations in the mid-IR, J. Quant. Spectrosc. Radiat. Transfer, 91, 275–285, 2005.

Höpfner, M., Ungermann, J., Borrmann, S., Wagner, R., Spang, R., Riese, M., Stiller, G., Appel, O., Batenburg, A. M., Bucci, S., Cairo, F., Dragoneas, A., Friedl-Vallon, F., Hünig, A., Johansson, S., Krasauskas, L., Legras, B., Leisner, T., Mahnke, C., Möhler, O., Molleker, S., Müller, R., Neubert, T., Orphal, J., Preusse, P., Rex, M., Saathoff, H., Stroh, F., Weigel, R., and Wohltmann, I.: Ammonium nitrate particles formed in upper troposphere from ground ammonia sources during Asian monsoons, Nature Geosciences, 12, 608–612, https://doi.org/10.1038/s41561-019-0385-8, 2019.

IPCC: Climate Change 2013: The Physical Science Basis. Contribution of Working Group I to the Fifth Assessment Report of the Intergovernmental Panel on Climate Change, Cambridge University Press, Cambridge, United Kingdom and New York, NY, USA, https://doi.org/10.1017/CBO9781107415324, 2013.

Kalicinsky, C., Griessbach, S., and Spang, R.: Radiative transfer simulations and observations of infrared spectra in the presence of polar stratospheric clouds: Detection and discrimination of cloud types, Atmos. Meas. Tech. Discuss., 2020, 1–28, https://doi.org/10.5194/amt-2020-144, 2020.

Keckhut, P., Hauchecorne, A., Bekki, S., Colette, A., David, C., and Jumelet, J.: Indications of thin cirrus clouds in the stratosphere at mid-latitudes, Atmos. Chem. Phys., 5, 3407–3414, 2005.

Kent, G. S., Winker, D. M., Vaughan, M. A., Wang, P. H., and Skeens, K. M.: Simulation of Stratospheric Aerosol and Gas Experiment (SAGE) II cloud measurements using airborne lidar data, J. Geophys. Res., 102, 21 795–21 807, https://doi.org/10.1029/97JD01390, 1997.

Kleinert, A., Friedl-Vallon, F., Guggenmoser, T., Höpfner, M., Neubert, T., Ribalda, R., Sha, M., Ungermann, J., Blank, J., Ebersoldt, A., Kretschmer, E., Latzko, T., Oelhaf, H., Olschewski, F., and Preusse, P.: Level 0 to 1 processing of the imaging Fourier transform spectrometer GLORIA: generation of radiometrically and spectrally calibrated spectra, Atmos. Meas. Tech., 7, 4167–4184, https://doi.org/10.5194/amt-7-4167-2014, 2014.

Krisch, I., Ungermann, J., Preusse, P., Kretschmer, E., and Riese, M.: Limited angle tomography of mesoscale gravity waves by the infrared limb-sounder GLORIA, Atmos. Meas. Tech., 11, 4327–4344, https://doi.org/10.5194/amt-11-4327-2018, 2018.

Kunz, A., Konopka, P., Müller, R., Pan, L., Schiller, C., and Rohrer, F.: High static stability in the mixing layer above the extratropical tropopause, J. Geophys. Res., 114, D16 305, https://doi.org/10.1029/2009JD011840, 2009.

Kunz, A., Konopka, P., Müller, R., and Pan, L. L.: Dynamical tropopause based on isentropic potential vorticity gradients, J. Geophys. Res., 116, D01 110, https://doi.org/10.1029/2010JD014343, 2011.

Liou, K.-N.: Influence of Cirrus Clouds on Weather and Climate Processes: A Global Perspective, Monthly Weather Review, 114, 1167–1199, https://doi.org/10.1175/1520-0493(1986)114<1167:IOCCOW>2.0.CO;2, 1986.

Luebke, A. E., Afchine, A., Costa, A., Grooß, J.-U., Meyer, J., Rolf, C., Spelten, N., Avallone, L. M., Baumgardner, D., and Krämer, M.: The origin of midlatitude ice clouds and the resulting influence on their microphysical properties, Atmos. Chem. Phys., 16, 5793–5809, https://doi.org/10.5194/acp-16-5793-2016, 2016.

Noël, V. and Haeffelin, M.: Midlatitude cirrus clouds and multiple tropopauses from a 2002–2006 climatology over the SIRTA observatory, J. Geophys. Res., 112, D13 206, https://doi.org/10.1029/2006JD007753, 2007.

Pan, L. L. and Munchak, L. A.: Relationship of cloud top to the tropopause and jet structure from CALIPSO data, J. Geophys. Res., 116, D12 201, https://doi.org/10.1029/2010JD015462, 2011.

Riese, M., Kaufmann, and M., Hoor, P.: WISE: project description, https://www.halo.dlr.de/science/missions/wise/wise.html, 2017, last accessed: 13 August 2020.

Riese, M., Ploeger, F., Rap, A., Vogel, B., Konopka, P., Dameris, M., and Forster, P.: Impact of uncertainties in atmospheric mixing on simulated UTLS composition and related radiative effects, J. Geophys. Res., 117, D16 305, https://doi.org/10.1029/2012JD017751, 2012.

Riese, M., Oelhaf, H., Preusse, P., Blank, J., Ern, M., Friedl-Vallon, F., Fischer, H., Guggenmoser, T., Hoepfner, M., Hoor, P., Kaufmann, M., Orphal, J., Ploeger, F., Spang, R., Suminska-Ebersoldt, O., Ungermann, J., Vogel, B., and Woiwode, W.: Gimballed Limb Observer for Radiance Imaging of the Atmosphere (GLORIA) scientific objectives, Atmos. Meas. Tech., 7, 1915–1928, https://doi.org/10.5194/amt-7-1915-2014, 2014.

Sassen, K. and Cho, B. S.: Subvisual-thin cirrus lidar data set for satellite verification and climatological research, J. Appl. Met., 31, 1275–1285, 1992.

Sassen, K., Wang, Z., and Liu, D.: Global distribution of cirrus clouds from CloudSat/Cloud-Aerosol Lidar and Infrared Pathfinder Satellite Observations (CALIPSO) measurements, J. Geophys. Res., 113, D00A12, https://doi.org/10.1029/2008JD009972, 2008.

Sembhi, H., Remedios, J., Trent, T., Moore, D. P., Spang, R., Massie, S., and Vernier, J. P.: MIPAS detection of cloud and aerosol particle occurrence in the UTLS with comparison to HIRDLS and CALIOP, Atmos. Meas. Tech., 5, 2537–2553, https://doi.org/10.5194/amt-5-2537-2012, 2012.

Spang, R., Riese, M., and Offermann, D.: CRISTA-2 observations of the south polar vortex in winter 1997: A new dataset for polar process studies, Geophys. Res. Lett., 28, 3159–3162, https://doi.org/10.1029/2000GL012374, 2001.

Spang, R., Hoffmann, L., Kullmann, A., Olschewski, F., Preusse, P., Knieling, P., Schroeder, S., Stroh, F., Weigel, K., and Riese, M.: High resolution limb observations of clouds by the CRISTA-NF experiment during the SCOUT-O3 tropical aircraft campaign, Adv. Space Res., 42, 1765–1775, https://doi.org/10.1016/j.asr.2007.09.036, 2008.

Spang, R., Arndt, K., Dudhia, A., Höpfner, M., Hoffmann, L., Hurley, J., Grainger, R. G., Griessbach, S., Poulsen, C., Remedios, J. J., Riese, M., Sembhi, H., Siddans, R., Waterfall, A., and Zehner, C.: Fast cloud parameter retrievals of MIPAS/Envisat, Atmos. Chem. Phys., 12, 7135–7164, https://doi.org/10.5194/acp-12-7135-2012, 2012.

Spang, R., Günther, G., Riese, M., Hoffmann, L., Müller, R., and Griessbach, S.: Satellite observations of cirrus clouds in the Northern Hemisphere lowermost stratosphere, Atmos. Chem. Phys., 15, 927–950, https://doi.org/10.5194/acp-15-927-2015, 2015.

Spang, R., Hoffmann, L., Höpfner, M., Griessbach, S., Müller, R., Pitts, M. C., Orr, A. M. W., and Riese, M.: A multi-wavelength classification method for polar stratospheric cloud types using infrared limb spectra, Atmos. Meas. Tech., 9, 3619–3639, https://doi.org/10.5194/amt-9-3619-2016, 2016.

Ungermann, J.: On Quantifying and Mitigation GLORIA Instrument Effects and Uncertainties, 2020, in preparation.

Ungermann, J., Blank, J., Lotz, J., Leppkes, K., Hoffmann, L., Guggenmoser, T., Kaufmann, M., Preusse, P., Naumann, U., and Riese, M.: A 3-D tomographic retrieval approach with advection compensation for the air-borne limb-imager GLORIA, Atmos. Meas. Tech., 4, 2509 – 2529, https://doi.org/10.5194/amt-4-2509-2011, 2011.

Ungermann, J., Blank, J., Dick, M., Ebersoldt, A., Friedl-Vallon, F., Giez, A., Guggenmoser, T., Höpfner, M., Jurkat, T., Kaufmann, M., Kaufmann, S., Kleinert, A., Krämer, M., Latzko, T., Oelhaf, H., Olchewski, F., Preusse, P., Rolf, C., Schillings, J., and Riese, M.: Level 2 processing for the imaging Fourier transform spectrometer GLORIA: Derivation and validation of temperature and trace gas volume mixing ratios from calibrated dynamics mode spectra, Atmos. Meas. Tech., 8, 2473–2489, https://doi.org/10.5194/amt-8-2473-2015, 2015.

Ungermann, J., Bartolome, I., Grießbach, S., Spang, R., Rolf, C., Krämer, M., Höpfner, M., and Riese, M.: Cirrus cloud shape detection by tomographic extinction retrievals from infrared limb emission sounder measurements, Atmos. Meas. Tech. Discuss., 2020, 1–35, https://doi.org/10.5194/amt-2020-256, 2020.

https://doi.org/10.5194/amt-2020-394
Preprint. Discussion started: 26 October 2020

Atmospheric Measurement Techniques Discussions

Weinreb, M. P. and Neuendorffer, A. C.: Method to apply homogeneous-path transmittance models to inhomogenous atmospheres, J. Atmos. Sci., 30, 662–666, 1973.

Zou, L., Griessbach, S., Hoffmann, L., Gong, B., and Wang, L.: Revisiting global satellite observations of stratospheric cirrus clouds, Atmos. Chem. Phys., 20, 9939–9959, https://doi.org/10.5194/acp-20-9939-2020, 2020.